Supporting Information: Photodetachment and Electron Dynamics in 1-Butyl-1-Methyl-Pyrrolidinium Dicyanamide

Meghan N. Knudtzon and David A. Blank*

Department of Chemistry, University of Minnesota, Minneapolis, MN 55455, United States

E-mail: blank@umn.edu

Contents

1 A simple model of average distance

To provide a rough estimate of the "reach" of the initially delocalized electron, the radial distribution of quencher distances at a given concentration was modeled using Eq. 1.[S1]

$$P(r) = \frac{3}{\gamma}\left(\frac{r}{\gamma}\right)^2 e^{-\left(\frac{r}{\gamma}\right)^3} \tag{1}$$

In Eq. 1 $\gamma = \left(\frac{3}{4\pi N}\right)^{1/3}$, N is the number density, r is the center-to-center distance between nearest points, and the point are assumed to be randomly distributed. The model ignores the finite volume of the particles, but is assumed to be a reasonable estimate at low concentrations.

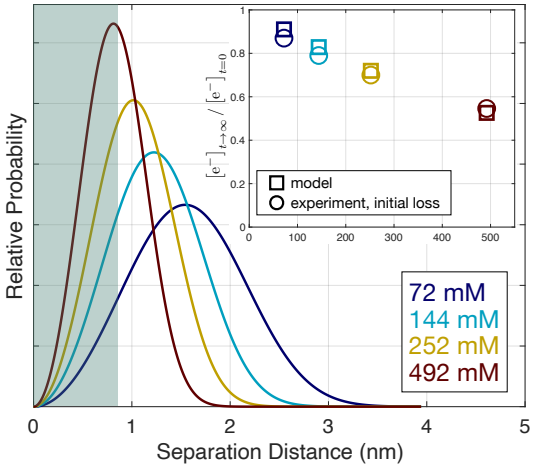

Figure S1: Average distance of a random distribution at a given concentration. The inset compares the fraction of the distribution below $r = 0.8$ nm (squares) to the fraction of the electrons lost during the initial localization event.

2 Stretched Exponential Fit for Geminate Recombination

The change in TA amplitude at a probe energy of 2.48 eV was fitted to Eq. 2 convoluted with a 200 fs FWHM Gaussian instrument response function.

$$S(t) = Ae^{-t/\tau_1} + Be^{-(t/\tau_2)^{\beta}} + Ce^{-t/\tau_3}. \tag{2}$$

The data and fit are presented in Fig. S2 with the fitting parameters given in Table S1. Two exponential decays were used to fit the rapid loss of signal at early times and the slowest component at the largest delay times. A third exponential decay was required to fit the loss of signal between 1 and 50 ps, with a stretched exponential decay providing a statistically better fit than a simple exponential decay.

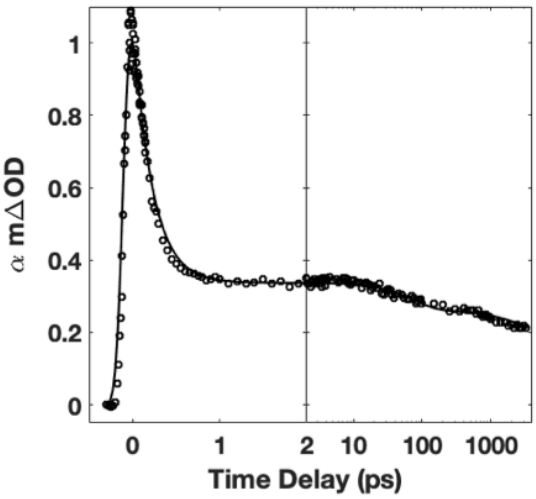

Figure S2: Transient absorption for $[Pyr^{+}_{1,4}][DCA^{-}]$ probed at 2.48 eV following excitation at 4.6 eV. The open circles are the data and the solid line is the fit using Eq. 2 with parameters given in Table S1.

Table S1: Parameters for fit given in Eq. 2 for evolution of signal at 2.48 eV, presented in Fig. S2.

A	τ_1 (fs)	B	τ_2 (ps)	β	C	τ_3 (ns)
0.770	217	0.050	75	1.34	0.180	14.76
± 0.015	± 8	± 0.01	± 28	± 1.12	± 0.008	± 7.26

3 Stretched Exponential Fit for E_{max}

The Heavyside function was used to offset the fit at 2 ps. A minimum of two exponential rises were required to obtain a reasonable fit and the fit was statistically improved by replacing one of the exponential rises with a stretch exponential rise. Shifting prior to 2 ps is largely dominated by the localization of the delocalized electron and is not quantitatively discussed here. Instead, our focus is on the solvation of the localized free electron.

$$S(t) = H + A(1 - e^{-t/\tau_1}) + B(1 - e^{(-t/\tau_2)^\beta}). \tag{3}$$

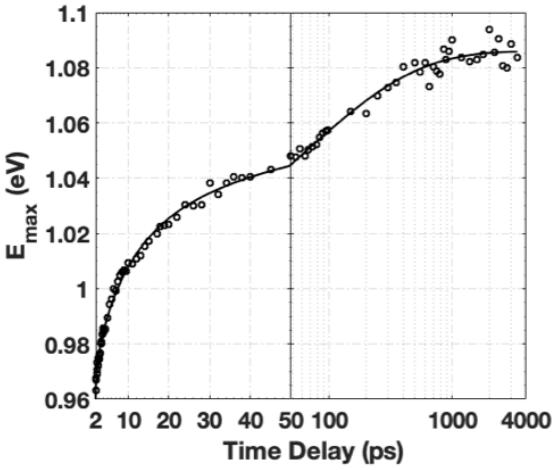

Figure S3: Energy at the maximum absorption, $E_{\max}$, as a function of delay time. The open circles are the data and the solid line is the fit using Eq. 3 with parameters given in Table S2.

Table S2: Fit parameters for evolution of maximum peak energy given by Eq. 3 and presented in Fig. S2.

H (eV)	A (eV)	τ_1 (ps)	B (eV)	τ_2 (ps)	β
0.9608	0.0233	9.059	0.102	59.71	0.459
±0.0020	± 0.0042	± 1.565	±0.006	±7.97	±0.262

4 Single Value Decomposition Analysis of near-IR pump-probe

The spectral signatures of each species in the near-IR, the initial delocalized excited state and the subsequent cavity localized electron, should undergo continuous evolution throughout the time delay probed. As a result, our hypothesis was that a global analysis decomposing the transient spectra into a set of static components with time dependent amplitudes would not reveal additional insights. In order to test this hypothesis we performed single value decomposition (SVD) analysis on the near-IR data show in Fig. 2 of the manuscript. We note that the transient spectra in the visible demonstrated very little change in shape throughout the time probed, and as a result there was no dynamic information available beyond the change in amplitude analysed in the manuscript.

The SVD results are presented in Fig. S4. The first principle component is the dominant component and shows a broad absorption across the near-IR that is nearly time independent. The second principle component is roughly anti-diagonal crossing the origin near the middle, and it appears to largely account for the the shift in the absorption spectrum to higher energy with time. In order to compare the time evolution of this component with the time evolution of the energy of maximum absorption (Figs. 5 and 6 in the manuscript), we fitted the time evolution of principle component 2 to the same equation as the data in Fig. 6.

$$a(t)S_a \xrightarrow{k_1} b(t)S_b \xrightarrow{k_2} c(t)S_c \xrightarrow{k_3} d(t)S_d \xrightarrow{k_4} e(t)S_e \tag{4}$$

The initial rate coefficient was set at $1/k_1 = 0.3$ ps based on the fastest rate observed in the

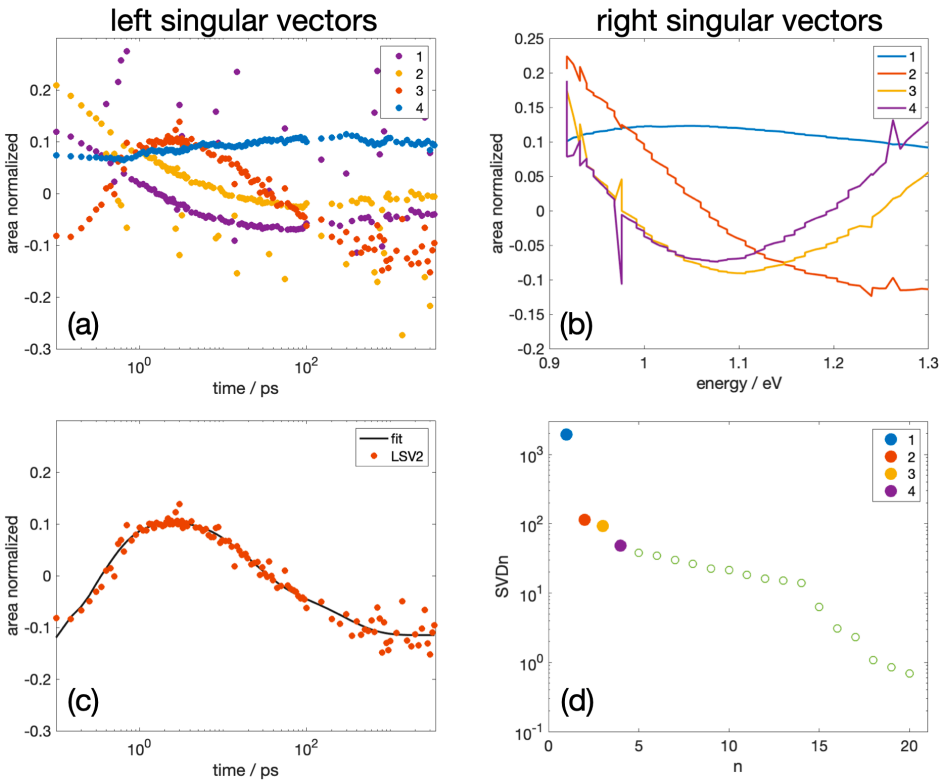

Figure S4: SVD analysis of the near-IR pump-probe data. (a) The left singular vectors (time), (b) the corresponding right singular vectors (energy), (d) is the SVDn amplitude for the individual singular vectors, and (c) the time evolution of the second principle component and the fit using Eq. 4 with parameters given in Table S3.

quenching fits, and the rest of the rate coefficients were fixed at the optimized values from the fits to the maximum absorption energy in Table 2. Only the amplitudes, S_A–S_E, were adjusted. The resulting fit parameters are presented in Table S3.

Table S3: Fit parameters for evolution of the second principle component using Eq. 4 and presented in Fig. S4(c). The time constants were fixed at the values from Table 2 of the manuscript, and the amplitudes (S_A–S_E) were optimized.

$1/k_1$ (ps)	$1/k_2$ (ps)	$1/k_3$ (ps)	$1/k_4$ (ps)	S_A	S_B	S_C	S_D	S_E
0.3	2.0	21.0	272	-0.197	0.088	0.11	-0.024	-0.11

The resulting fit shown is Fig. S4(c) demonstrates that the dynamics captured in the SVD analysis are the same dynamics (based on time scales) that were captured in Figs. 5 and 6 of the manuscript. Given that this reflects the shifting in the transient absorption spectrum rather than the change in population of a species with a static transient spectrum, we have chosen to leave the analysis of the shift in the energy of maximum absorption in the manuscript as a more intuitive measure.

Principle components 3 and 4 are smaller contributions and appear to be associated with the change in shape of the spectrum with time, primarily a narrowing. The rest of the singular vectors appear to account for more subtle changes in the shape of the energy spectrum, and become increasingly noisy as the amplitude becomes small.

Overall, we found that the analysis confirmed our initial hypothesis. SVD did not provide significant additional insight into the measured transient spectra in this case.

5 Fit to near-IR amplitude at 1.13 eV

The lifetime of the free electron was determined by fitting the change in amplitude of the signal at a probe energy of 1.13 eV as a function of delay time, presented in Fig. S5. The data

was fitted to a stretched exponential rise and exponential decay, given by Eq. 5, convoluted with a 200 fs FWHM Gaussian instrument response function.

$$S(t) = A(1 - e^{-(t/\tau_1)^{\beta}}) + Be^{-t/\tau_2}. \tag{5}$$

The optimized fitting parameters are given in Table S4. Inclusion of the stretched exponential rise statistically improved the quality of the fit over the use of a simple exponential rise. The initial rise at 1.13 eV reflects shifting of the absorption spectrum of the electrons as they relax. The lifetime of the free electron obtained from this fit was 20 $\pm$7 ns. While it far exceeds the 3.5 ns maximum delay accessible in our experiment and carries significant uncertainty, the lifetime is consistent with radiolysis reports of free electron surviving for hundreds of nanoseconds in other ionic liquids. However, this time constant shows the lifetime of the solvated electron exceeds the other dynamics examined in this study.

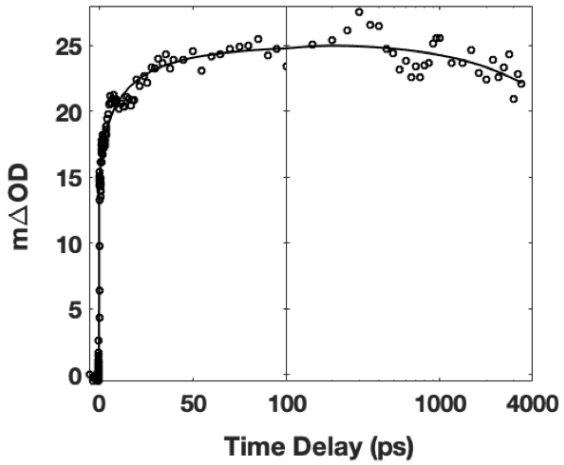

Figure S5: Transient absorption in $[Pyr^{+}_{1,4}][DCA^{-}]$ excited at 4.6 eV and probed at 1.13 eV. The open circles are the data and the fit (solid line) is given by Eq. 5 with parameters in Table S4.

Table S4: Fit parameters for the evolution of signal at 1.13 eV.

A (mΔOD)	τ_1 (ps)	β	B (mΔOD)	τ_2 (ns)
10.75 ± 0.71	11.75 ± 1.61	0.636 ± 0.08	14.24 ± 0.56	20.82 ± 7.17

6 Exponential fit to DCM quenching

The electron scavenging dynamics for a series of DCM concentrations were fitted to the sum of an exponential decay and a stretched exponential decay, Eq. 6. The parameters of the fit are presented in Table S5. For the lowest concentration of DCM, 24 mM, the signal-to-noise was not sufficient to capture the dynamics of the fast exponential decay.

$$S(t) = Ae^{-t/\tau_1} + Be^{-(t/\tau_2)^{\beta}} \tag{6}$$

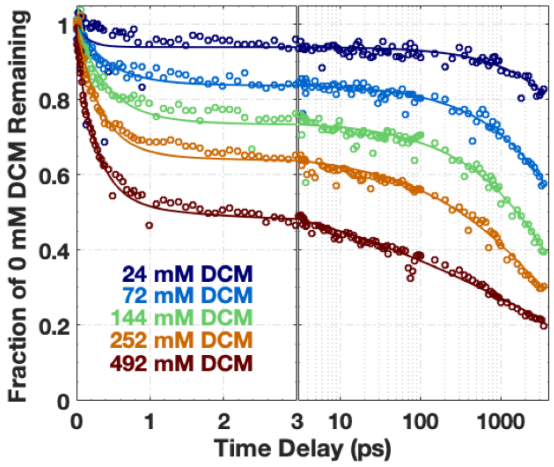

Figure S6: Fraction of signal remaining at 1.13 eV compared to neat $[Pyr^{+}_{1,4}][DCA^{-}]$ for various concentrations of DCM. The open circles are the data and the fit (solid line) is given by Eq. 6 with parameters in Table S5.

Table S5: Optimized fitting parameters using Eq. 6 to fit the DCM quenching data measured at 1.13 eV in Fig. S6. The 68.2% confidence interval determined when all variables are simultaneously optimized is given below each value.

[DCM] (mM)	A	τ_1 (fs)	B	β	τ_2 (ns)
24	–	–	0.939	0.735	48.51
	–	–	± 0.004	± 0.084	± 16.68
72	0.160	431	0.841	0.616	17.21
	± 0.005	± 39	±0.002	±0.037	± 2.24
144	0.259	425	0.741	0.582	7.96
	± 0.008	± 34	±0.003	± 0.044	± 0.89
252	0.340	325	0.661	0.445	5.55
	± 0.02	±47	±0.002	± 0.02	± 0.31
492	0.390	271	0.611	0.212	2.74
	±0.006	±16	± 0.003	±0.018	± 0.41

References

(S1) Mean Inter-Particle Distance. https://en.wikipedia.org/w/index.php?title=Mean_inter-particle_distance&oldid=965441291, 2020.